



1 **High-resolution elevation mapping of the McMurdo Dry**
2 **Valleys, Antarctica and surrounding regions**

3 Andrew G. Fountain¹, Juan C. Fernandez-Diaz², Maciej Obryk¹, Joseph Levy³, Michael
4 Gooseff⁴, David J. Van Horn⁵, Paul Morin⁶, and Ramesh Shrestha²

5 ¹Department of Geology Portland State University, Portland, OR 97201, USA

6 ²National Center for Airborne Laser Mapping, University of Houston, Houston, TX 77204, USA

7 ³University of Texas, Institute for Geophysics, Jackson School of Geosciences, Austin, TX 78758, USA

8 ⁴Institute of Arctic & Alpine Research, University of Colorado, Boulder, CO, 80309

9 ⁵Department of Biology, University of New Mexico, Albuquerque, NM 87131

10 ⁶Polar Geospatial Center, University of Minnesota, St. Paul, MN 55108, USA

11 *Correspondence to:* Andrew G. Fountain (andrew@pdx.edu)

12

13 **Abstract**

14 We present detailed surface elevation measurements for the McMurdo Dry Valleys,
15 Antarctica derived from aerial lidar surveys flown in the austral summer of 2014-2015 as part
16 of an effort to understand geomorphic changes over the past decade. Lidar return density
17 varied from 2 to >10 returns m⁻² with an average of about 5 returns m⁻². vertical and
18 horizontal accuracies are estimated to be 7 cm and 3 cm, respectively. In addition to our
19 intended targets, other ad hoc regions were also surveyed including the Pegasus flight facility
20 and two regions on Ross Island, McMurdo Station, Scott Base (and surroundings), and the
21 coastal margin between Cape Royds and Cape Evans. These data are included in this report
22 and data release. The combined data is freely available at doi: 10.5069/G9D50JX3.

23

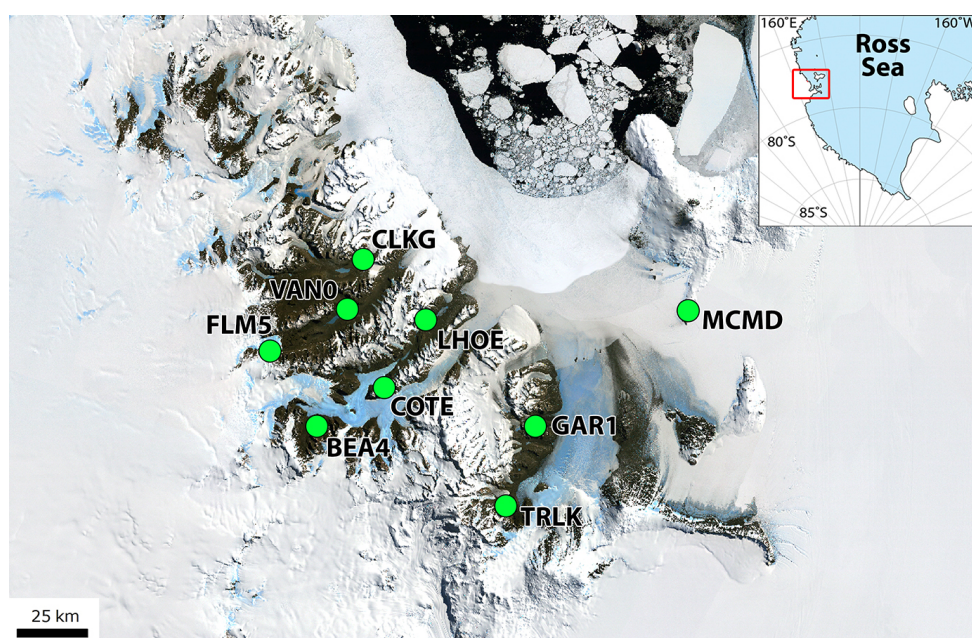
24 **1. Introduction**

25 The McMurdo Dry Valleys (MDV) are a polar desert located along the Ross Sea coast of
26 East Antarctica (~77.5°, ~162.5° E S; Figure 1). These valleys are not covered by the East
27 Antarctic ice sheet due to the blockage to flow by the Transantarctic Mountains and the
28 severe rain-shadow caused by these mountains (Chinn, 1981; Fountain et al., 2010). The
29 valleys are a mosaic of gravelly-sandy soil, glaciers, ice-covered lakes and ephemeral melt
30 streams that flow from the glaciers. Permafrost is ubiquitous with active layers up to 75 cm
31 deep (Bockheim et al., 2007). This region is of interest to geologists and biologists. It is one
32 of the few regions in Antarctica with exposed bedrock from which the tectonic history of the



33 continent can be explored (Gleadow and Fitzgerald, 1987; Marsh, 2004). The bare landscape
34 also provides evidence for past glaciations, a critical observatory into the past behavior of the
35 Antarctic Ice Sheet (Brook et al., 1993; Denton and Hughes, 2000; Hall et al., 2010). The
36 cold dry environment of the MDV host an unusual terrestrial habitat dominated by microbial
37 life (Adams et al., 2006; Cary et al., 2010) and serves as a useful terrestrial analogue for
38 Martian conditions (Kounaves et al., 2010; Levy et al., 2008; Samarkin et al., 2010).

39



40

41 Figure 1. Landsat image mosaic of Antarctica, LIMA (Bindschadler et al., 2008), map of the central
42 McMurdo Dry Valleys with locations of UNAVCO fixed global positioning system ground stations.

43 Over the last decade the topography of the coastal margins have been changing due to
44 melting of subsurface deposits of massive ice (Bindschadler et al., 2008; Fountain et al.,
45 2014). For example, the Garwood River in Garwood Valley has rapidly eroded through ice-
46 cemented permafrost and buried massive ice sometime after December 2000 (Levy et al.,
47 2013, p.2). In Taylor Valley, observations in 2014-15 along Commonwealth Stream showed a
48 similar erosive behavior. Other streams in Taylor Valley, including Crescent, Lost Seal, and
49 Lawson, have exhibited recent bank undercutting (Gooseff et al., 2015). Over the 50+ years
50 of observations these changes are the first of their kind. Also, we have observed glacier



51 thinning where significant sediment deposits have collected on the surface (Fountain et al.,
52 2015).

53 Common to all changes is the occurrence of a relatively thin veneer of sediment over massive
54 ice. In the case of the valley floor the sediment veneer is $\sim 10^{-1}$ m in thickness whereas on the
55 glaciers it is patchy with thicknesses of $\sim 10^{-3}$ to 10^{-2} m. In addition, anecdotal observations
56 point to large changes in other stream channels, and increasing roughness and perhaps
57 thinning of the lower elevations of some glaciers.

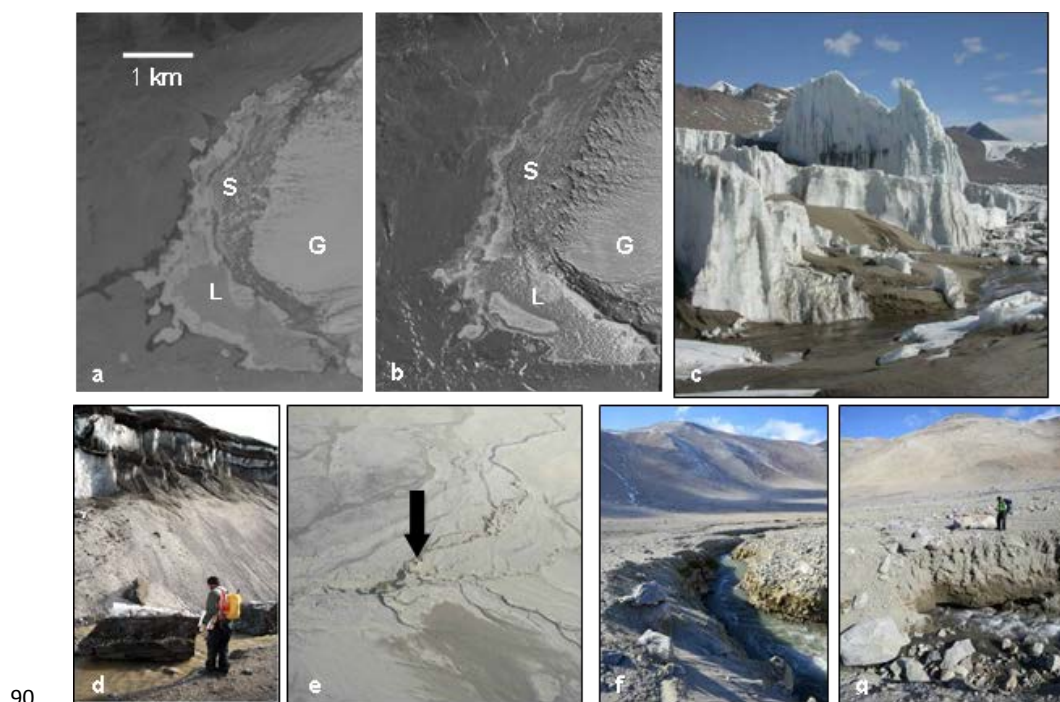
58 To assess the magnitude and spatial distribution of landscape changes the valleys were
59 surveyed using a high resolution airborne topographic lidar during the austral summer of
60 2014-2015 and the results were compared to an earlier survey flown in the summer of 2001-
61 2002 (Csatho et al., 2005; Schenk et al., 2004). Our working hypothesis is that landscape
62 change is limited to the 'coastal thaw zone' where maximum summer temperatures exceed -
63 5°C (Fountain et al., 2014; Marchant and Head, 2007). Here we summarize the field
64 campaign of 2014-2015, data processing, and the point cloud of elevation data covering about
65 $3,300\text{ km}^2$ of the MDV, and 264 km^2 of areas of interest nearby, all of which have been made
66 openly available to the research community.

67 **2. Approach**

68 In early December 2014, the lidar personnel from the National Science Foundation's National
69 Center for Airborne Laser Mapping (NCALM) and the science team from Portland State
70 University arrived in McMurdo Station for an eight-week field season. Two airborne laser
71 scanner (ALS) instruments were used in the survey. The main instrument was the Titan MW,
72 a newly designed multispectral ALS based on performance specifications provided by
73 NCALM. with an integrated digital camera manufactured for NCALM by Teledyne Optech,
74 Inc, Toronto, Canada. It is the first operational ALS designed to perform mapping using three
75 different wavelengths simultaneously through the same scanning mechanism (Fernandez-
76 Diaz et al., 2016a, 2016b). Two wavelengths are in the near-infrared spectrum (1550 and
77 1064 nm) and the third in the visible (532 nm). This three-wavelength capability enables the
78 Titan MW to map elevations of solid ground (topography) and depths below water surface
79 (bathymetry – but not available for reasons described later) simultaneously. This three-
80 channel spectral information can be combined into false-color laser backscatter images,
81 which improves the ability to distinguish between types of land cover. The system is mounted



82 under the aircraft, scanning side-to-side at an angle of up to ± 30 -degrees off-nadir, producing
83 a saw-tooth ground pattern. The 1064 nm channel points at nadir and the 1550 and 532 nm
84 channel point 3.5° and 7° forward of nadir, respectively. Each channel can acquire up to
85 300,000 measurements per second. However, the nominal operation pulse repetition rate for
86 the MDV survey was 100 kHz per channel. For some extreme regions where the terrain relief
87 was extremely high the Titan MW had to be operated at lower pulse rates of 75 and 50 kHz.
88 For each pulse the Titan only records first, second, third and last returns. The Titan scanner
89 was operated at an angle of $\pm 30^\circ$ and a frequency of 20 Hz.



90

91 Figure 2. Examples of ice-mediated elevation changes in the McMurdo Dry Valleys. Disintegration of
92 the lower ablation zone of the Wright Lower Glacier, Wright Valley, (a) 1980; (b) 2008. S - sediment-
93 covered part of the glacier, G - relatively clean part of the glacier, L - Lake Brownworth. The dots just
94 below the S in the 2008 photo are ice spires several meters tall with sediment-covered ablated ice
95 surrounding it, depicted in (c), photo: M. Sharp; (d) Ice cliff exposed by the eroding Garwood River;
96 (e) Aerial view of Garwood River incision and bank collapse. River flows right to left. Arrow points to
97 the where photos f and g are taken; (f) Recent incision, note color differences; (g) The river has
98 carved a thermokarst tunnel.



99 The advantage of Titan MW over traditional ALS systems for mapping regions like the MDV
100 where areas of soil and snow overlap is the multiple channels at different wavelengths. A
101 traditional ALS operating at 1550 nm obtains strong returns from the soil surfaces but may
102 have difficulties over ice and snow, which reflect less at that wavelength. The additional
103 1064- and 532-nm channels have a better response to snow. Also, three channels collecting
104 data simultaneously increases the data density compared to single channel units. However, a
105 limitation of the Titan system is the maximum ranging of $\sim \leq 2$ km.

106 The second ALS was an Optech Gemini ALTM, which served as a backup to the Titan MW.
107 The Gemini ALTM is a single channel system that uses 1064 nm laser pulses at repetition
108 frequencies of 33 to 166 kHz and it can scan a swath of up to $\pm 25^\circ$ off nadir. While the
109 returns densities obtained with the Gemini are lower than that from the Titan MW system, it
110 has the advantage of a longer maximum range $\sim \leq 4$ km. The Gemini was operated at pulse
111 rate frequency between 70 and 100 kHz, its scanner ran at $\pm 25^\circ$ and a frequency of 35 Hz, its
112 beam divergence was set at 0.25 milliradians.

113 The DiMAC Ultralight camera, integrated in the Titan MW system acquires digital vertical
114 aerial photographs during the laser scanning and together they can produce digital
115 orthophotographs. The camera uses a charged coupled device (CCD) with 60 megapixels,
116 each with a dimension of $6 \mu\text{m} \times 6 \mu\text{m}$. The pixels are arranged in an array of 8,984 pixels
117 oriented perpendicular to the flight direction and 6,732 pixels along the flight direction,
118 which translate to CCD physical chip size of 5.39 cm x 4.04 cm. The image is formed on the
119 focal plane through a compound lens with a focal length of 70 mm. The combination of lens
120 and CCD array yields a total field-of-view (FOV) of $42.1^\circ \times 32.2^\circ$ and a ground sample
121 distance of $0.0000825 \times$ flight height (~ 5 cm for nominal mission altitudes of 600 meters
122 above ground level. The position of the CCD is adjusted during flight through a piezo
123 actuator to compensate for the motion of the aircraft during an exposure reducing pixel
124 smear.

125 To derive accurate differential kinematic trajectories for the ALS a total of nine UNAVCO
126 global positioning system (GPS) stations were used as reference, recording data at a rate of 1
127 Hz (Figure 1). This network of GPS stations provided sufficient coverage to ensure that the
128 aircraft was no more than 40 km from any station during mapping operations.

129

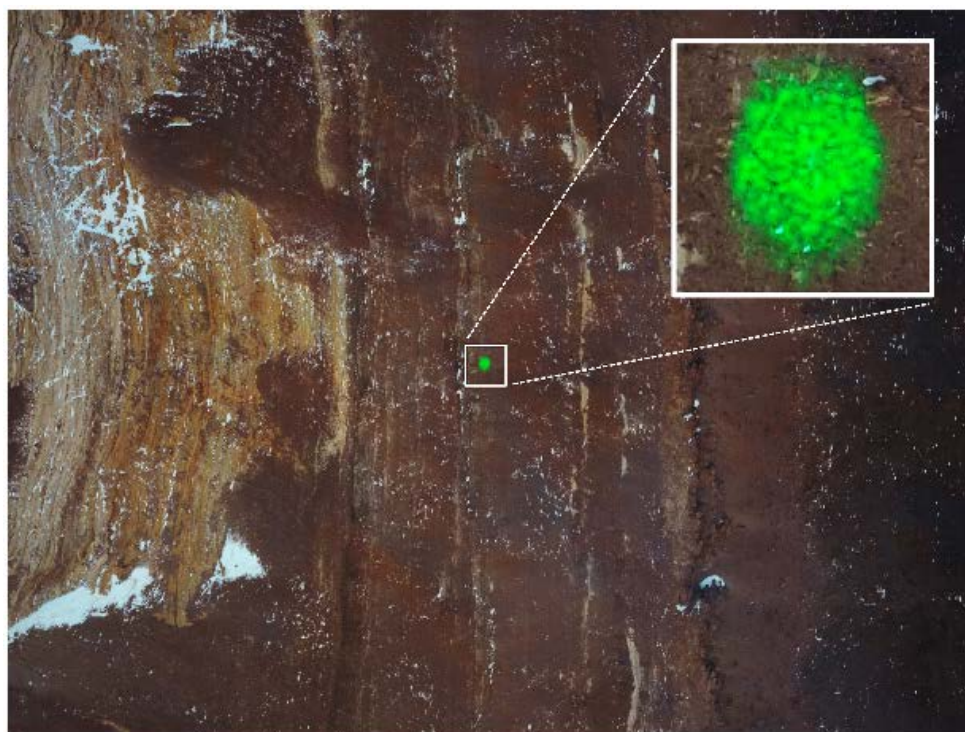
130



131 **3. Results from the Field Campaign**

132 The Titan MW ALS was mounted within a DHC-6 Twin Otter aircraft operated by Ken
133 Borek Air, of Calgary, Canada under contract to the National Science Foundation. The
134 aircraft flew at a nominal speed of $65 - 70 \text{ m s}^{-1}$ at a nominal flight height of 600 m above the
135 surface (actual flight heights above terrain ranged between 400 and 2500 m). The footprint of
136 the lasers beam was about 0.3 m for channels 1 and 2 and about 0.6 m for channel 3 (Figure
137 3).

138



139

140 Figure 3. Image of the titan channel 3 (532 nm) laser footprint captured by the digital camera over
141 the floor of Wright valley.

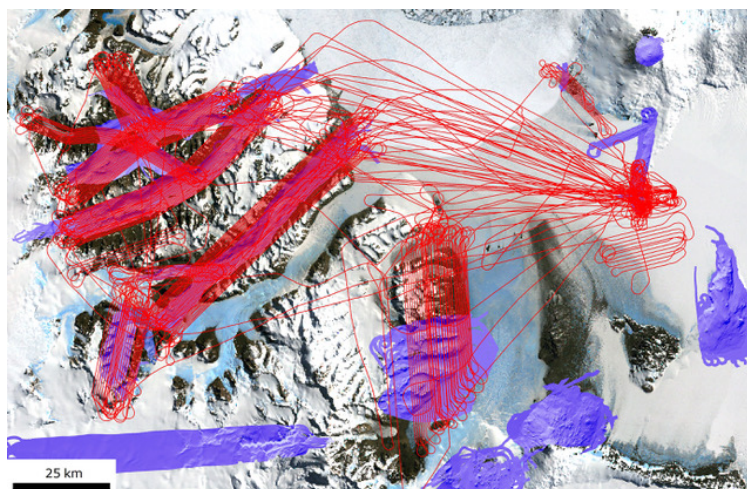
142

143 The aerial survey was planned to cover the entire 5000 km^2 of the MDV but adverse weather
144 conditions prevented complete coverage (flight days vs. deployment days). Fortunately, the
145 prioritized valley bottoms and regions previously scanned by NASA in 2001 were surveyed
146 and none of our science objectives were compromised. Occasionally, the priority MDV



147 targets were unavailable during flight operations and nearby ad hoc regions of opportunity
148 were surveyed, including McMurdo Station and surroundings, Pegasus Airfield, and the
149 coastal area between and including Cape Royds and Cape Evans. These ad hoc regions,
150 together with the MDV, totaled about 3600 km² from which 3564 km² of elevations rasters
151 were produced of surveyed landscape (Figure 4).

152 Reliability of the Titan MW system was good with only one day lost due to an intermittent
153 malfunction. A total of 109 aircraft engine-on hours were used, of these 94.7 hours were
154 flying hours which yielded a total of 50.9 laser-on hours (47.4 hours with Titan MW and 3.4
155 hours with Gemini). A total of 42.5 billion laser shots were fired, of which about two-thirds
156 (28.7 billion) produced usable returns. The unusable returns were primarily due to a
157 saturation of channel 3 (532 nm) of the Titan system. This channel is optimized for weak
158 returns to enhance the ability to see through clear water. However, the detector was
159 overwhelmed by sunlight reflections off the steep valley walls and multipath reflections
160 produced by the highly reflective snow and ice. This caused the detector to trigger spurious
161 returns saturating the ability of the sensor to record actual surface returns. The remaining
162 usable returns were equally divided between channels 1 and 2. Returns from the outer 5° of
163 either side of the swath (scan angle cut-off) were also discarded to reduce scan line artifacts.



164

165

166 Figure 4. Flight lines for the new 2014-2015 survey shown in red over the extent of the 2001 survey
167 shown in purple digital elevation model hillshades. Base map is the Landsat Image Mosaic of
168 Antarctica (Bindschadler et al., 2008).



169 Survey patterns were described as ‘mowing the lawn’ as the plane flew back and forth along
170 the longitudinal axis of each valley with the goal of 50% overlap with the prior swath such
171 that the edge of the newly acquired swath overlaps from the edge to the center of the adjacent
172 previously-flown swath. The separation between the flight lines was ~350 m. Due to adverse
173 weather 50% lateral swath overlap was not always possible.

174 After the aircraft landed, preliminary processing was performed to examine the coverage and
175 identify gaps to be re-flown. The time between initial and final coverage depended on
176 weather. While the performance of Titan MW met most of its design parameters it was not
177 able to detect usable returns in the deeper parts of Taylor Valley because the safe flight height
178 above local terrain exceeded the range limit of the instrument. To survey these regions, the
179 Gemini sensor was installed towards the end of the flying season and the data gaps were
180 closed. The resulting spatial point density of the laser returns varied due to differences in
181 flight height, weather, and repeat coverage to close gaps (Figure 5). Overall, the range of
182 unfiltered laser returns varied from 2 returns m^{-2} to >10 returns m^{-2} , with an average of 4.7
183 returns m^{-2} .

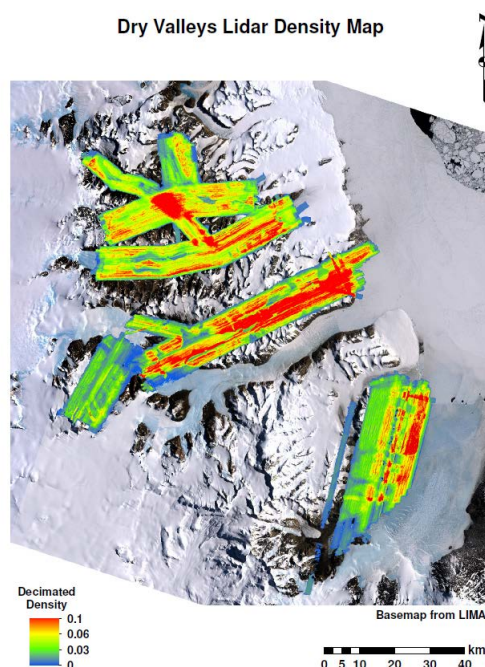
184

185 Figure 5. Return density map for the
186 2013-2014 lidar survey of the McMurdo
187 Dry Valleys. The units of density are
188 returns $\text{m}^{-2} \times 10$. Base map is the Landsat
189 Image Mosaic of Antarctica (Bindschadler
190 et al., 2008)

191

192 4. Final Data Processing

193 After returning from Antarctica the
194 data were processed in four main steps:
195 trajectory determination, point cloud
196 production, point cloud processing,
197 and elevation raster generation. The
198 first step was to produce accurate
199 differential trajectories for the aircraft. Initially, the three-dimensional coordinates for
200 aircraft (sensor) position were derived from the GPS stations using the KARS (Kinematic and





201 Rapid Static) software (Mader, 1996) taking data from one GPS station at a time. For each
202 flight its final trajectory in three dimensions was derived by blending solutions from at least
203 three GPS stations. These data were then combined with orientation information collected
204 from the Inertial Measurement Unit, operating at 200 kHz. We used a Kalman Filter
205 algorithm within POSPac Mobile Mapping Suite Version 7.1 (Applanix, Corp), to combine
206 these data. The final navigation solution obtained is known as a ‘Smoothed Best Estimated
207 Trajectory’ (SBET) and resulted in a binary file containing the sensor’s position and
208 orientation.

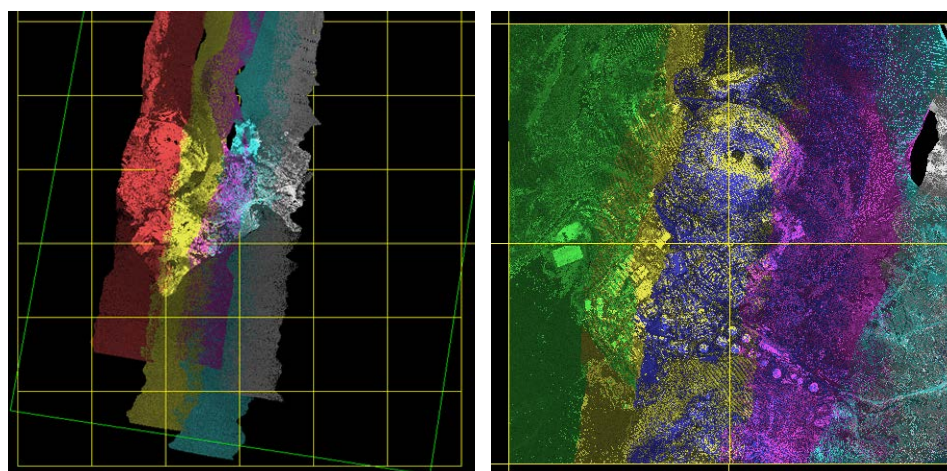
209 The second processing step, point cloud production, combined the laser range data with the
210 SBET to produce geo-located point clouds of laser returns. The point cloud production was
211 performed with the sensor manufacturer’s proprietary software LMS for the Titan MW and
212 Dashmap for the Gemini. Before producing the point cloud for the entire project area a small
213 subset of the cloud was carefully examined. This geographical subset was selected before the
214 data were collected to serve as a calibration and validation (CAL/VAL) site. The CAL/VAL
215 site has structural and topographic features that allowed for verifying that all systematic
216 sources of error that can affect the geometric and geolocation quality of the returns were
217 accounted for. The calibration or boresight adjustment of an ALS ensured that returns were
218 consistent with each other (within same and different flight lines) and reduced data artifacts.
219 The point clouds obtained for the CAL/VAL area were visually and analytically checked and
220 parameters were adjusted to improve the geometric quality of the returns when the point
221 cloud was regenerated. Through this iterative process the calibration was refined to obtain a
222 final set of calibration parameters that were applied to the range data for the entire project to
223 produce the point clouds of each flight line. Each data return was positioned in three-
224 dimensional space by horizontal coordinates in US Geological Survey Transantarctic
225 Mountains Projection (epsg projection 3294) and vertical coordinate in meters above the
226 World Geodetic Survey 1984 (WGS84) ellipsoid.

227 Besides the geolocation information, each return contains information regarding the strength
228 of the backscattered energy (intensity), and the GPS time for the emission of the laser pulse.
229 The point clouds are encoded following the American Society of Photogrammetry and
230 Remote Sensing (ASPRS) LAS 1.2 laser return file format (.las). The point clouds produced
231 for each flight line are referred to as strips (Figure 6a). Because of complexity of some strips,
232 their size, and overlap with adjacent strips, for simplicity in handling and further processing



233 the strips were combined and the coverage re-organized into orthogonal tiles of dimension 1
234 km x 1 km as illustrated in Figure 6.

235



236

237

a.

b.

238 Figure 6. Lidar point cloud strips and point cloud tiles illustrating how a large coverage area is broken
239 down into tiles. (a) Five flight strips over McMurdo Station, the strip point clouds have been
240 rendered based on flight line and intensity. The yellow grid represents the 1 km x 1km tiles into
241 which the returns from the different strips will be binned into. (b) Point clouds for four tiles. The
242 tiled point clouds are rendered based on flight line and intensity. The overlap between the different
243 flight strips within each tile is evident on this rendering.

244 Once the point cloud was organized into tiles the final step removed atmospheric noise,
245 multipath returns, and outlier returns using a combination of automated algorithms and
246 manual editing. Data from overlapping flight lines within a given tile might have been
247 collected on different flights and because the vertical GPS trajectory solution may vary
248 within a few decimeters it was necessary to adjust the elevation of each flight strip to remove
249 any possible bias. Elevation adjustments were performed with Terrasolid Terramatch
250 software. For each tile Terramatch compared the elevations of the different flight lines within
251 common coverage areas and computes vertical adjustment values for each flight line. In
252 addition to ensuring consistency between elevations of different flight lines, this process can
253 be tied to control points with well-known elevations such that the adjusted elevations are also
254 consistent with a given vertical datum. After adjusting for these vertical offsets the final point

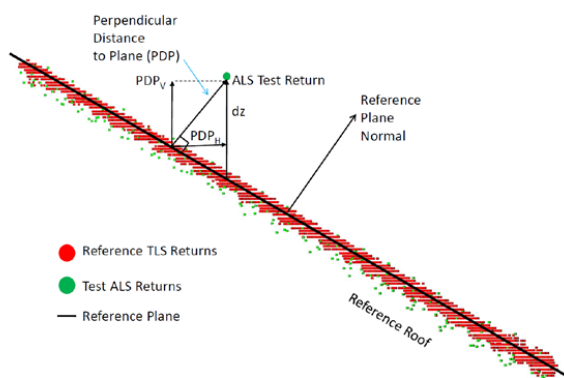


255 cloud tiles were produced. Of the 28.7 billion adequate returns from the MDV, about 50%
 256 were discarded due to the $\pm 5^\circ$ swath edge cut-off and to noise removal resulting in a total of
 257 14.1 billion returns in the final point clouds.

258 The accuracy of the geolocation of the laser returns was verified against a terrestrial laser
 259 scanning (TLS) data of buildings and structures from McMurdo Station which was collected
 260 by Merrick and Company. Planar building roofs were selected as reference. A plane was
 261 fitted to the TLS data of a roof using the linear least squares method and the difference in
 262 elevation (dz) and perpendicular distance to plane were computed for respective airborne
 263 returns for the same planar roof surfaces (Figure 7). The advantage of this method over the
 264 traditional methods of collecting kinematic GPS measurements over flat uniform surfaces
 265 such as roads, runways (Heidemann, 2014) is that it permits decomposition of the accuracy in
 266 both horizontal and vertical components. A total of 35 planes were employed for the accuracy
 267 assessment consisting of almost 560,000 TLS measurements and a total of 5008 airborne
 268 lidar returns.

269 The RMSE for the distance to plane measurement was 7.6 cm with a vertical and horizontal
 270 component RMSE of 6.9 cm and 3.2 cm respectively. It is important to make two critical
 271 observations regarding these values. First, this method might provide higher RMSE values
 272 than the traditional method because the geolocation of the TLS dataset has positional
 273 uncertainties higher than a vehicle kinematic survey which is generally used as reference
 274 dataset for the traditional method. Second, the horizontal uncertainty is probably an
 275 underestimate, and while it represents an average value under constrained conditions (low
 276 airplane dynamics, 600 m range) the horizontal uncertainty can be as high as 20-30 cm under
 277 more unfavorable flight conditions.

278
 279 Figure 7. Illustration of assessing
 280 uncertainty for airborne lidar
 281 survey (ALS) compared to
 282 terrestrial lidar survey (TLS) of an
 283 inclined roof.



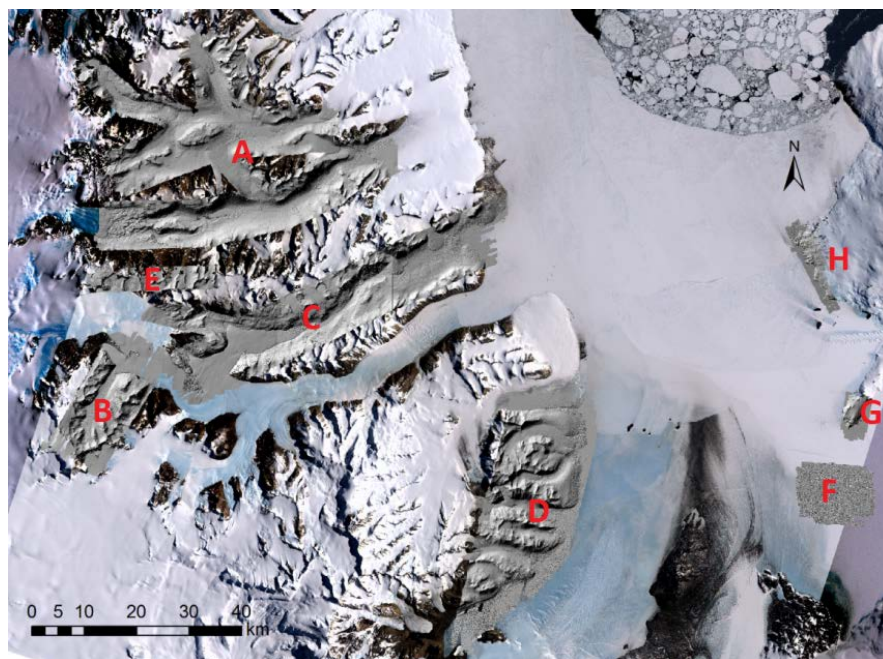
284

285



286 With the finalized point clouds, irregularly spaced data were interpolated, using Kriging
287 methods, to a regularly spaced grid at 1 m intervals forming the digital elevation models
288 (DEM). The algorithm was applied to each tile and included returns 10 m into the
289 neighboring tiles to avoid tile boundary artefacts. The tiles were mosaicked into large
290 coverage rasters (~400 km²) and converted into ArcGIS elevation rasters. The gridding,
291 mosaicking, and conversion of the digital elevation models was performed using Surfer
292 software (Golden Software, Golden, CO). The ArcGIS elevation rasters were used to produce
293 shaded relief images of the valleys images with standard illumination parameters: Azimuth
294 315°, elevation 45°, Z factor 1 (Figure 8)

295



296

297 Figure 8. Shaded relief maps of the McMurdo Dry Valleys based on aerial lidar surveys conducted
298 from December to January 2014-2015. A. are the northern valleys of Victoria, Barwick, McKelvey and
299 Wright with adjacent valleys; B. is Beacon Valley and surroundings; C. is Taylor Valley and
300 surroundings; and D. is the southern Dry Valleys of Garwood, Miers, Marshall, and adjacent valleys.
301 E) is a section of the Asgard ranges. F) Pegasus Field. G) McMurdo Station area. H. Capes Royds and
302 Evans. Base map is the Landsat Image Mosaic of Antarctica (Bindschadler et al., 2008).

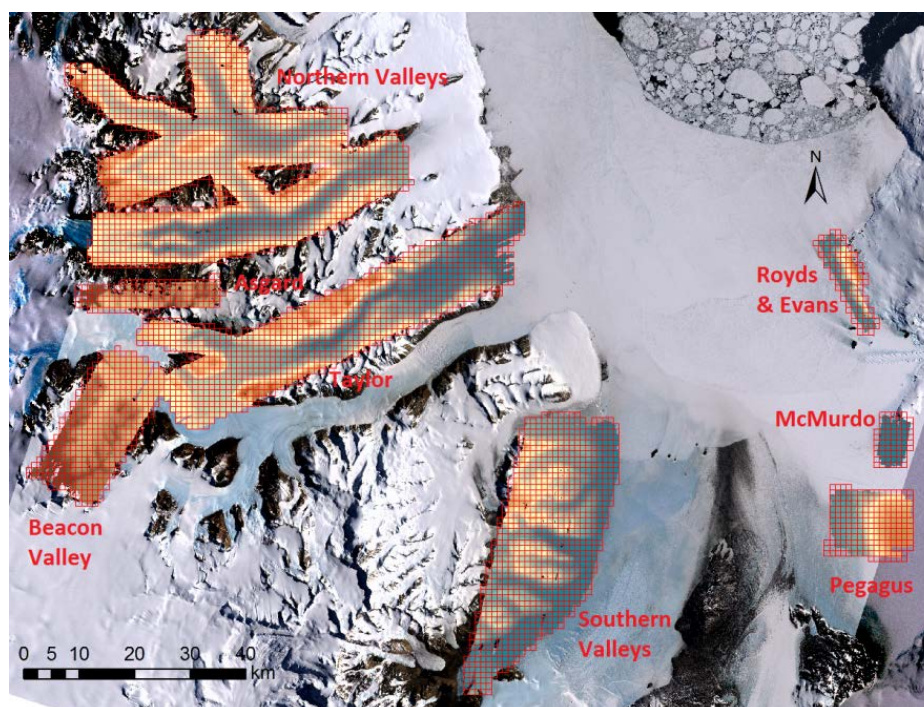
303



304 5. Data Products

305 Three types of data products derived from the lidar survey are available. Spatial coverage for
306 these products includes: five regions within the McMurdo Dry Valleys (Figure 9, 1) Taylor
307 Valley, which also includes Pearse Valley; 2) The Northern valleys, which include Wright,
308 McKelvey, Balham, Barwick, and the Victoria valleys; 3) Southern valleys, which include
309 Garwood, Marshall and Miers valleys and surrounding areas; 4) Beacon Valley; 5) a section
310 of the Asgard Range; and three ad hoc regions, 1) Pegasus aviation facility; 2) McMurdo
311 Station and surroundings; and 3) the coastal margin from Capes Royds to Cape Evans. The
312 lidar data products include, clean point clouds in a 1 km x 1km tiles in the ASPRS .las
313 format, DEMs in the ESRI ArcGIS .flt format and shaded relief maps in the ESRI ArcGIS
314 .adf format. The ArcGIS rasters have a horizontal resolution of 1 m. Specifics related to the
315 extent and file size of these data products for each of the surveys areas are summarized in
316 Table 1.

317



318

319 Figure 9. Map showing the location and extent of the available lidar data products. Base map is the
320 Landsat Image Mosaic of Antarctica (Bindschadler et al., 2008).



321 Table 1: Summary of available lidar data products. Returns are the lidar returns from the Earth's surface;
 322 # of LAS Tiles, is the number of point cloud tiles for each section; LAS Gb, is the data storage size in
 323 gigabytes for the point cloud data; # of Sections, are the number of individual section that constitute the
 324 entire elevation raster for each region; DEM Gb, is the data storage size in gigabytes of the digital
 325 elevation model that covers that region; and SRM Gb, is the data storage size in gigabytes of the shaded
 326 relief maps.

327

Region	Coverage Area km ²	Point cloud products			Elevation Rasters		
		Returns x10 ⁶	# LAS Tiles	LAS Gb	# Sections	DEM Gb	SRM Gb
Taylor	852.8	4,112.5	944	107.0	3	6.8	1.0
Northern	1,289.8	5,417.2	1447	141.0	3	10.1	1.6
Southern	755.1	2,800.7	827	73.0	2	5.5	0.9
Beacon Valley	316.1	651.4	376	16.9	1	3.1	0.4
Asgard Range	94.8	129.5	136	3.4	1	0.7	0.1
Pegasus	157.8	504.3	181	13.1	1	0.9	0.1
McMurdo	42.3	257.9	59	6.7	1	0.3	0.1
Royds & Evans	63.4	253.3	92	6.6	1	0.9	0.1

328

329 6. Data availability

330 The data products in this report can be obtained from two different National Science Foundation
 331 funded data facilities, Open Topography, www.opentopography.org, the webpage hosting the data
 332 can be found at <https://doi.org/10.5069/G9D50JX3>, and the Polar Geospatial Center www.pgc.umn.edu.

333 7. Summary

334 We have compiled a high resolution elevation dataset for 3564 km² of the McMurdo Dry
 335 Valleys, Antarctica, focused largely (but not exclusively) on the valley bottoms. These new
 336 data, with a return density of averaging 5 returns m⁻² improve the raster DEM quality,
 337 compared to the lidar survey flown in 2002 (Shenk et al., 2004) by a factor of 4, from 2 m² to
 338 1 m². We also include an estimate of uncertainties based on detailed terrestrial lidar surveys
 339 of building roofs at McMurdo Station collected independently from our investigation. This
 340 approach differs from the traditional method of a vehicle-mounted GPS unit driven over a flat
 341 surface of a road by using inclined surfaces yielding both vertical and horizontal
 342 uncertainties. Comparing the elevations of 35 inclined building roofs our RSME uncertainty
 343 is ±0.07 m in the vertical and ±0.03 m in the horizontal. However, we recognize that the
 344 horizontal uncertainty may be as much as an order of magnitude higher due to poor flight
 345 conditions. In addition to the primary mission of the project we also surveyed nearby regions
 346 including the Pegasus aviation facility on the McMurdo Ice Shelf, and two localities on Ross



347 Island, the region covering McMurdo Station and Scott Base, and the coastal margin from
348 Cape Royds to Cape Evans. Data products include point clouds provided in a 1 km x 1 km
349 tiles, 1 m resolution digital elevation models (DEMs) and shaded relief maps.

350 **8. Author contribution**

351 All authors contributed to the drafting and editing of the manuscript. Andrew Fountain was
352 the principle investigator of the project, writing the proposal and working in the field with the
353 NCALM group flying the lidar. He helped to examine the final data quality and led the
354 writing of this report. Juan Fernandez-Diaz was lead for the aerial lidar survey, coordinating
355 the flights, instrument operations, data production and performing final data quality
356 assessments and verifications. He also wrote major sections of this report. Maciej Obryk lead
357 the field campaign to deploy the GPS receivers for the aircraft and worked on the data quality
358 issues. Joseph Levy was a co-PI of the project and helped with data quality issues. Michael
359 Gooseff and David Van Horn were co-PIs of the project. Paul Morin helped design the
360 project, provided logistical and technical support for the crew on the field (deploy GPS
361 receivers) and during data processing. Ramesh Shrestha help organize the lidar and field
362 strategy and coordinated among the PIs and funding agency.

363 **9. Acknowledgements**

364 The GPS units and data were provided by the polar operations group of UNAVCO and we
365 particularly acknowledge Joe Pettit and for making this operation easy and efficient.
366 Members of the Polar Geospatial Center aided us in the deployment and collection of the
367 GPS units. The pilots and support staff of Kenn Borek Air Ltd, were great to work with,
368 showed much patience in flying endless flight lines, and kept to the desired trajectory despite
369 unexpected turbulence. The NCALM personnel responsible for the collection and processing
370 of lidar and imagery data for this project include Abhinav Singhanian, Darren Hauser, and
371 Michael Sartori. Matt Bethel, Director of Operations and Technology and Erick Mena Sr.
372 Laser Scanning Technician of Merrick & Company provided terrestrial laser scanning data of
373 McMurdo Station that was used for accuracy assessment of the airborne lidar data. And all
374 the people that make working and living at McMurdo Station, Antarctica possible. This work
375 was supported by NSF Antarctic Integrated Systems Science award ANT-1246342 to AGF.



376 **References**

- 377 Adams, B. J., Bardgett, R. D., Ayres, E., Wall, D. H., Aislabie, J., Bamforth, S., Bargagli, R.,
378 Cary, C., Cavacini, P., Connell, L., Convey, P., Fell, J. W., Frati, F., Hogg, I. D., Newsham,
379 K. K., O'Donnell, A., Russell, N., Seppelt, R. D. and Stevens, M. I.: Diversity and
380 distribution of Victoria Land biota, *Soil Biol. Biochem.*, 38(10), 3003–3018,
381 doi:10.1016/j.soilbio.2006.04.030, 2006.
- 382 Bindschadler, R. A., Vornberger, P., Fleming, A., Fox, A. D., Mullins, J., Binnie, D.,
383 Paulsen, S., Granneman, B. and Gorodetzky, D.: The Landsat image mosaic of Antarctica,
384 *Remote Sens. Environ.*, 112(12), 4214–4226, doi:10.1016/j.rse.2008.07.006, 2008.
- 385 Bockheim, J. G., Campbell, I. B. and McLeod, M.: Permafrost distribution and active-layer
386 depths in the McMurdo Dry Valleys, Antarctica, *Permafr. Periglac. Process.*, 18(3), 217–227,
387 doi:10.1002/ppp.588, 2007.
- 388 Brook, E. J., Kurz, M. D., Ackert, Jr., R. P., Denton, G. H., Brown, E. T., Raisbeck, G. M.
389 and Yiou, F.: Chronology of Taylor Glacier advances in Arena Valley, Antarctica, using in
390 situ cosmogenic ^3He and ^{10}Be , *Quat. Res.*, 39, 11–23, 1993.
- 391 Cary, S. C., McDonald, I. R., Barrett, J. E. and Cowan, D. A.: On the rocks: the microbiology
392 of Antarctic Dry Valley soils, *Nat. Rev. Microbiol.*, 8(2), 129–138, doi:10.1038/nrmicro2281,
393 2010.
- 394 Chinn, T. J. H.: Hydrology and climate in the Ross Sea area, *J. R. Soc. N. Z.*, 11(4), 373–386,
395 doi:10.1080/03036758.1981.10423328, 1981.
- 396 Csatho, B., Schenk, T., Krabill, W., Wilson, T., Lyons, G. M., Hallam, C., Manizade, S. and
397 Paulsen, T.: Airborne laser scanning for high-resolution mapping of Antarctica, *Eos*, 86(25),
398 237–238, 2005.
- 399 Denton, G. H. and Hughes, T. J.: Reconstruction of the Ross ice drainage system, Antarctica,
400 at the last glacial maximum, *Geogr. Ann. Ser. Phys. Geogr.*, 82(2–3), 143–166, 2000.
- 401 Fernandez-Diaz, J., Carter, W., Glennie, C., Shrestha, R., Pan, Z., Ekhtari, N., Singhania, A.,
402 Hauser, D. and Sartori, M.: Capability Assessment and Performance Metrics for the Titan
403 Multispectral Mapping Lidar, *Remote Sens.*, 8(11), 936, doi:10.3390/rs8110936, 2016a.
- 404 Fernandez-Diaz, J. C., Carter, W. E., Shrestha, R. and Glennie, C. L.: Multicolor terrain
405 mapping documents critical environments, *EOS Trans. Am. Geophys. Union*, 97,
406 doi:10.1029/2016EO053489, 2016b.
- 407 Fountain, A. G., Nysten, T. H., Monaghan, A., Basagic, H. J. and Bromwich, D.: Snow in the
408 McMurdo Dry Valleys, Antarctica, *Int. J. Climatol.*, (30), 633–642, doi:10.1002/joc.1933,
409 2010.
- 410 Fountain, A. G., Levy, J. S., Gooseff, M. N. and Van Horn, D.: The McMurdo Dry Valleys:
411 A landscape on the threshold of change, *Geomorphology*,
412 doi:10.1016/j.geomorph.2014.03.044, 2014.



- 413 Gleadow, A. J. W. and Fitzgerald, P. G.: Uplift history and structure of the Transantarctic
414 Mountains: new evidence from fission track dating of basement apatites in the Dry Valleys
415 area, southern Victoria Land, *Earth Planet. Sci. Lett.*, 82, 1–14, 1987.
- 416 Gooseff, M. N., Van Horn, D., Sudman, Z., McKnight, D. M., Welch, K. A. and Lyons, W.
417 B.: Biogeochemical and suspended sediment responses to permafrost degradation in stream
418 banks in Taylor Valley, Antarctica, *Biogeosciences Discuss.*, 12(17), 14773–14796,
419 doi:10.5194/bgd-12-14773-2015, 2015.
- 420 Hall, B. L., Denton, G. H., Fountain, A. G., Hendy, C. H. and Henderson, G. M.: Antarctic
421 lakes suggest millennial reorganizations of Southern Hemisphere atmospheric and oceanic
422 circulation, *Proc. Natl. Acad. Sci.*, 107(50), 21355–21359, 2010.
- 423 Heidemann, H. K.: Lidar base specification (ver. 1.2, November 2014), 2014.
- 424 Kounaves, S. P., Stroble, S. T., Anderson, R. M., Moore, Q., Catling, D. C., Douglas, S.,
425 McKay, C. P., Ming, D. W., Smith, P. H., Tamppari, L. K. and Zent, A. P.: Discovery of
426 Natural Perchlorate in the Antarctic Dry Valleys and Its Global Implications, *Environ. Sci.*
427 *Technol.*, 44(7), 2360–2364, doi:10.1021/es9033606, 2010.
- 428 Levy, J. S., Head, J. W., Marchant, D. R. and Kowalewski, D. E.: Identification of
429 sublimation-type thermal contraction crack polygons at the proposed NASA Phoenix landing
430 site: Implications for substrate properties and climate-driven morphological evolution,
431 *Geophys. Res. Lett.*, 35(4), doi:10.1029/2007GL032813, 2008.
- 432 Levy, J. S., Fountain, A. G., Dickson, J. L., Head, J. W., Okal, M., Marchant, D. R. and
433 Watters, J.: Accelerated thermokarst formation in the McMurdo Dry Valleys, Antarctica, *Sci.*
434 *Rep.*, 3, 2, doi:10.1038/srep02269, 2013.
- 435 Mader, G. L.: Kinematic and rapid static (KARS) GPS positioning: Techniques and recent
436 experiences, in *GPS trends in precise terrestrial, airborne, and spaceborne applications*, pp.
437 170–174, Springer, Berlin., 1996.
- 438 Marchant, D. R. and Head, J. W.: Antarctic dry valleys: Microclimate zonation, variable
439 geomorphic processes, and implications for assessing climate change on Mars, *Icarus*, 192(1),
440 187–222, doi:10.1016/j.icarus.2007.06.018, 2007.
- 441 Marsh, B.: A magmatic mush column rosetta stone: the McMurdo Dry Valleys of Antarctica,
442 *Eos Trans. Am. Geophys. Union*, 85(47), 497–502, 2004.
- 443 Samarkin, V. A., Madigan, M. T., Bowles, M. W., Casciotti, K. L., Priscu, J. C., McKay, C.
444 P. and Joye, S. B.: Abiotic nitrous oxide emission from the hypersaline Don Juan Pond in
445 Antarctica, *Nat. Geosci.*, 3(5), 341–344, doi:10.1038/ngeo847, 2010.
- 446 Schenk, T., Csathó, B., Ahn, Y., Yoon, T., Shin, S. W. and Huh, K. I.: DEM generation from
447 the Antarctic LiDAR data: Site report, US Geol. Surv. [online] Available from:
448 [http://www.nsm.buffalo.edu/Research/rs1/research/DEM/presentations_papers/dryvalleys_at](http://www.nsm.buffalo.edu/Research/rs1/research/DEM/presentations_papers/dryvalleys_at_m_sitereport_v5_04sep.pdf)
449 [m_sitereport_v5_04sep.pdf](http://www.nsm.buffalo.edu/Research/rs1/research/DEM/presentations_papers/dryvalleys_at_m_sitereport_v5_04sep.pdf) (Accessed 1 July 2014), 2004.